



Cite this: *RSC Adv.*, 2018, 8, 3051

# Enhanced osteogenic activity of Ti alloy implants by modulating strontium configuration in their surface oxide layers

Zhengjiang Xu,<sup>†a</sup> Huaifeng Lu,<sup>†ab</sup> Jian Lu,<sup>b</sup> Chen Lv,<sup>b</sup> Xiaobing Zhao<sup>\*b</sup> and Guocheng Wang<sup>ID \*a</sup>

To guarantee the long-term stability of an orthopaedic implant, non-degradable surface coatings with the ability to selectively release bioactive drugs or ions are especially desirable. In this study, SrO–TiO<sub>2</sub> composite coatings were deposited on the surface of Ti alloys, whose release behavior of bioactive Sr ions was modulated by the Sr configurations, either interstitial atoms in solid solution (Ti<sub>y</sub>Sr<sub>2–2y</sub>O<sub>2</sub>) or strontium titanate (SrTiO<sub>3</sub>). A perfect linear relationship between the amount of the released Sr ions and the Sr content in the coating was observed. Among the SrO-doped TiO<sub>2</sub> coatings, the 20% SrO–TiO<sub>2</sub> coating where Sr existed in both forms of Ti<sub>y</sub>Sr<sub>2–2y</sub>O<sub>2</sub> and SrTiO<sub>3</sub> not only promoted proliferation of bone cells but also enhanced their osteogenic differentiation, which was proved to be related to its Sr release behavior. However, overdosing with 30% SrO only resulted in one single Sr configuration (SrTiO<sub>3</sub>) and an inferior osteogenic function. This study suggests that Sr configurations of both interstitial atoms of the solid solution and SrTiO<sub>3</sub> can realize the selective release of Sr, but they possibly have different effects on the biological functions and other properties including corrosion resistance.

Received 30th September 2017  
 Accepted 4th January 2018

DOI: 10.1039/c7ra10807a

[rsc.li/rsc-advances](http://rsc.li/rsc-advances)

## 1. Introduction

A variety of metal ions have been documented to be essential for the human body and widely used as therapeutic agents in the treatment of many types of diseases, such as anemia, bone, brain and neuron diseases.<sup>1–3</sup> In bone tissue engineering, some metal ions, represented by strontium (Sr),<sup>4</sup> zinc (Zn),<sup>5</sup> magnesium (Mg)<sup>6</sup> *etc.* were proven to promote bone tissue regeneration and have been widely used in the field of therapeutic tissue engineering. One of the most important advantages of using metal ions is that it does not pose risks of decomposition or instability, which are intrinsic to some drugs and proteins.<sup>3,7</sup> Among those ions reported to be essential for bone metabolism, Sr has been demonstrated to stimulate bone regeneration and inhibit bone resorption,<sup>8–10</sup> which has raised great interest in construction of osteoinductive bone biomaterials.

Titanium and its alloy are the most commonly used implant materials for dental and orthopaedic applications due to their good mechanical properties, biocompatibility and corrosion resistance.<sup>11,12</sup> However, they cannot achieve sufficient

functional integration (osseointegration) with the surrounding bone to establish a firm and long-lasting anchor, as the implant surface lacks osteoinductivity. Therefore, surface activation is required to obtain a satisfactory long-term performance.<sup>13,14</sup> Benefiting from the osteogenic function of Sr ions, they have been used by various methods to activate Ti alloy implant surface.<sup>15–18</sup> The commonest way is to introduce Sr in a biodegradable material that can be deposited onto the implant surface *via* a certain of surface techniques.<sup>19–21</sup> Upon degradation of the material, the Sr ions release and the resultant biological effects on bone cells can be realized.<sup>16</sup> However, since the bone implant is supposed to permanently stay in human body, the utilization of a biodegradable coating on its surface could risk the interfacial stability and probably cause implant aseptic loosening upon the coating absorption, if its degradation rate cannot match the new bone formation rate.<sup>22</sup> Therefore, to better use of the osteogenic benefits of Sr and avoid the risk of implant loosening caused by the coating degradation, a chemically stable surface coating with an ability to release Sr ions would be preferred.

In this study, we choose biocompatible and chemically stable TiO<sub>2</sub> as the main component of the surface coating material, which is supposed to permanently exist during the service time of the implant. Sr ions were incorporated into the TiO<sub>2</sub> promote the osseointegration of the implant. To modulate the ion release behavior, the amount of Sr in the TiO<sub>2</sub> was tailored in order to control the Sr configuration (Sr–TiO<sub>2</sub>) solid solution and strontium titanate (SrTiO<sub>3</sub>) in the composite

<sup>a</sup>Research Center for Human Tissues and Organs Degeneration, Shenzhen Institutes of Advanced Technology, Chinese Academy of Science, Shenzhen, Guangdong 518055, China. E-mail: [gc.wang@siat.ac.cn](mailto:gc.wang@siat.ac.cn)

<sup>b</sup>School of Materials Science and Engineering, Changzhou University, Changzhou 213164, China. E-mail: [zhaoxiaobing00@163.com](mailto:zhaoxiaobing00@163.com)

<sup>†</sup> Zhengjiang Xu and Huaifeng Lu are co-first authors, equally contributing to this article.



coating. The release of Sr is not associated with the degradation of the whole coating material, thus avoiding the risk of compromising the implant stability resulted from by the coating degradation. The ion release behavior, corrosion resistance and bioactivity of the Sr-doped coatings were evaluated and discussed.

## 2. Materials and methods

### 2.1. Coating fabrication

TiO<sub>2</sub> and SrO nanopowders were used as starting materials. 10% SrO-TiO<sub>2</sub>, 20% SrO-TiO<sub>2</sub> and 30% SrO-TiO<sub>2</sub> composite powders were produced by mixing using planetary ball mill. Coatings were deposited on biomedical grade Ti alloy (Baoji Junhang Metal Material Co., Ltd. Shanxi, China) with a diameter of 15 mm and 1 mm thickness by an atmospheric plasma spraying system (9M, Sulzer Metco, USA). Before plasma spraying, the Ti alloy substrates were ultrasonically cleaned in absolute ethanol and sandblasted with brown corundum. For cell culture experiments, the Ti alloy discs without any coatings and with pure TiO<sub>2</sub> coating were used as controls. The main parameters used in this study to prepare the TiO<sub>2</sub>, 10% SrO-TiO<sub>2</sub>, 20% SrO-TiO<sub>2</sub> and 30% SrO-TiO<sub>2</sub> coatings are listed as follows: spraying power was 42 kW, Ar flow rate was 40 L min<sup>-1</sup>, H<sub>2</sub> flow rate was 12 L min<sup>-1</sup>, spraying distance was 100 mm and powder feed rate was 30 g min<sup>-1</sup>.

### 2.2. Coating characterization

**2.2.1. X-ray diffraction (XRD) and scanning electron microscopy (SEM).** The phase structures of the coatings were conducted by X-ray diffraction (XRD, D/max 2500PC, Rigaku, Japan) with Cu K $\alpha$  radiation ( $\lambda = 1.5418 \text{ \AA}$ ) in the range of 20–80° (2 $\theta$ ). Scanning electron microscopy (SEM, S-3400, Japan) was used to examine the surface morphology.

**2.2.2. Ion release profile.** The coatings were immersed in 1 mL of  $\alpha$ -minimum essential medium ( $\alpha$ -MEM, Hyclone, USA) (pH = 7.4) at 37 °C. The medium was refreshed every 3 d. At each time point (3, 6 and 9 days), the culture medium was collected for measurement. The ion concentration of Ti and Sr in the culture medium was measured by inductively coupled plasma atomic emission spectroscopy (ICP-OES).

**2.2.3. *In vitro* cell-free mineralization.** The as-sprayed TiO<sub>2</sub> and the SrO doped TiO<sub>2</sub> coatings were cleaned in an ultrasonic bath with ethanol and distilled water. Modified simulated body fluid (2 $\times$  SBF) with Ca and P ion concentrations double those in the normal simulated body fluid (SBF). The samples were soaked in the 2 $\times$  SBF at 37 °C for 14 d without stirring and the solution were refreshed every 7 days. The 2 $\times$  SBF solution containing 142.0 mmol L<sup>-1</sup> Na<sup>+</sup>, 5.0 mmol L<sup>-1</sup> K<sup>+</sup>, 1.5 mmol L<sup>-1</sup> Mg<sup>2+</sup>, 5.0 mmol L<sup>-1</sup> Ca<sup>2+</sup>, 148.5 mmol L<sup>-1</sup> Cl<sup>-</sup>, 4.2 mmol L<sup>-1</sup> HCO<sub>3</sub><sup>-</sup> and 2.0 mmol L<sup>-1</sup> HPO<sub>4</sub><sup>2-</sup> and 0.5 mmol L<sup>-1</sup> SO<sub>4</sub><sup>2-</sup> was prepared by dissolving the reagents of NaCl, NaHCO<sub>3</sub>, KCl, K<sub>2</sub>HPO<sub>4</sub>·H<sub>2</sub>O, MgCl<sub>2</sub>·6H<sub>2</sub>O, CaCl<sub>2</sub> and Na<sub>2</sub>SO<sub>4</sub> into distilled water. The 2 $\times$  SBF solution was buffered at pH 7.4 with Tris and HCl.<sup>23</sup>

**2.2.4. Electrochemical measurements.** The corrosion resistance of the coatings were measured by the Autolab electrochemical workstation (PGSTAT 302N, METROHM, Swiss) in SBF solution using a three-electrode configuration comprising an Ag/AgCl electrode as the reference electrode, a platinum rod as the counter electrode, and the sample as the working electrode. The measurements were performed at room temperature with a scanning rate of 5 mV s<sup>-1</sup>. The corrosion rate was calculated based on the following equation.<sup>24</sup>

$$\text{Corrosion rate} = \frac{0.13\Delta I_{\text{corr}}\Delta EW}{d} \quad (1)$$

### 2.3. Biological test

**2.3.1. Cell culture and seeding.** Rats bone marrow mesenchymal stem cells (rBMSCS) was isolated from SD rat bone marrow. SD rats were purchased from Guangdong Medical Laboratory Animal Center (Guangzhou, China). Briefly, bone marrow was rinsed out with complete culture medium consisting of  $\alpha$ -MEM, 10% fetal bovine serum (FBS, Gibco, USA) and 1% antibiotics (100  $\mu\text{g mL}^{-1}$  gentamycin and 100 U mL<sup>-1</sup> penicillin). When reaching 80–90% confluence, cells were digested by 0.25% trypsin, collected by centrifugation and diluted to the desired density in culture medium. 1 mL of cell suspension with a density of  $2 \times 10^4$  cells per cm<sup>2</sup> was added onto each samples placed in 24-well cell culture plates. The medium was refreshed every two days.

**2.3.2. Initial cellular attachment.** To evaluate the cell attachment, cells were cultured on the samples for 24 h, and then were fixed with 2.5% glutaraldehyde in 30 min. For SEM, cell were washed with PBS twice and then dehydrated in gradient ethanol solution with final drying by isoamyl acetate. For immunofluorescent staining, the fixed cells were permeabilized with 0.1% (v/v) Triton X-100 for 7 min, and the unspecific staining was blocked by incubation in 1% BSA for 30 min. For focal adhesion staining, the specimens were incubated overnight at 4 °C with 2  $\mu\text{g mL}^{-1}$  of mouse anti-mouse vinculin primary antibody (Abcam, UK) diluted in 1% BSA/PBS solution. After three washes, the sample was then incubated for 1 h with 2  $\mu\text{g mL}^{-1}$  of goat anti-mouse IgG H&L (Alexa Fluor® 647) (Abcam, UK). The actin cytoskeleton was labeled by Phalloidin-FITC (Sigma, USA) for 45 min, and the cell nucleus was stained by 4',6-diamidino-2-phenylindole dihydro-chloride (DAPI, Sigma, USA) for 5 min. The stained cells were observed under the fluorescence microscope (OLYMPUS-BX53, Japan).

**2.3.3. Cell proliferation.** Cell Viability Kit-8 (CCK-8, Beyotime, China) was used to evaluate the cell proliferation on the coated Ti alloys. After incubation for 3 and 7 days, culture medium was removed and replaced by 10% CCK-8 working solution, followed by 2 h incubation. The OD values at 450 nm were read by a multi-well plate reader (Thermo Scientific Multiskan GO, Thermo).

**2.3.4. Alkaline phosphates (ALP) activity assay.** For alkaline phosphatase (ALP) activity evaluation, after 14 days' incubation, the medium was removed from the cell culture plates and washed with PBS twice, followed by 30 min incubation in 200  $\mu\text{L}$  of 1% Triton X-100 solution containing 100 mM



Table 1 Primer sequences for polymerase chain reaction

| Gene   | Sequences (5'-3')                                     |
|--------|---|
| RUNX-2 | F:ATCCAGCCACCTTCACTTACACC<br>R:GGGACCATTGGGAAGTATAGG  |
| COL-1  | F:CTGCCAGAAAGATATGTATCACC<br>R:GAAGCAAAGTTTCTCCAAGACC |
| OPN    | F:GACGGCCGAGGTGATAGCTT<br>R:CATGGCTGGTCTTCCCGTTGC     |
| OCN    | F:GCCCTGACTGCATTCTGCCTCT<br>R:TCACCACCTTACTGCCCTCCTG  |
| GAPDH  | F:GGCACAGTCAAGGCTGAGAATG<br>R:ATGGTGGTGAAGACGCCAGTA   |

phenylmethanesulfonyl fluoride (PMSF). Then 50  $\mu\text{L}$  of the cell lysates was transferred to a 96-well plate and incubated for 2 h at 37  $^{\circ}\text{C}$  with 200  $\mu\text{L}$  of *p*-nitrophenyl phosphate substrate solution (pNPP, Sigma, USA). ALP activity was quantified according to the absorbance at a wavelength of 405 nm. The total protein content in each cell lysate was determined using a BCA protein assay kit, to which ALP activity was normalized.

**2.3.5. Cell differentiation.** RBMSCs were seeded onto the Ti6Al4V, TiO<sub>2</sub> and the SrO doped TiO<sub>2</sub> coatings at density of  $2 \times 10^4$  cells per cm<sup>2</sup> and cultured for 7 and 14 days. The total RNA isolation and qPCR were performed strictly following the instruction from the assay kit provider. The forward and reverse primers of the selected genes are listed in Table 1. Detailed information about the experimental procedure can be found in our previous work.<sup>25</sup>

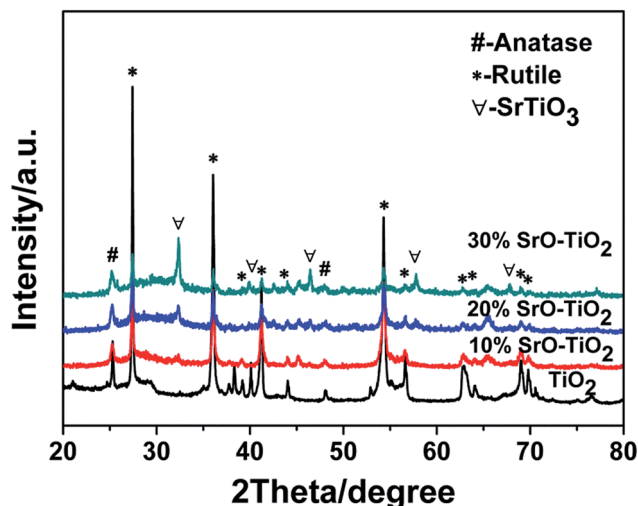
## 2.4. Statistical analysis

For statistical analysis, SPSS 17.0 program was used and the data were expressed as mean  $\pm$  SD. Levene's test was performed to determine the homogeneity of variance for all the data. Tukey HSD *post hoc* tests were used for the data with homogeneous variance. Tamhane's *T2 post hoc* was employed in the case that the tested group did not have a homogeneous variance. A *p*-value of less than 0.05 was considered significant.

## 3. Results

### 3.1. XRD analysis

Fig. 1 shows the XRD patterns of the TiO<sub>2</sub>, 10% SrO-TiO<sub>2</sub>, 20% SrO-TiO<sub>2</sub> and 30% SrO-TiO<sub>2</sub> coatings on Ti alloy substrates. In the diffraction pattern of the TiO<sub>2</sub> coating, peaks at  $2\theta$  values of 27.4 $^{\circ}$ , 36.1 $^{\circ}$ , 41.2 $^{\circ}$ , 54.3 $^{\circ}$  and 62.7 $^{\circ}$  are assigned to (110), (101), (111), (211) and (002) crystalline planes of rutile TiO<sub>2</sub>. For the doped TiO<sub>2</sub> coatings, the characteristic peaks of SrTiO<sub>3</sub> at 32.4 $^{\circ}$  and 39.9 $^{\circ}$  were found, and their intensity increases as the amount of SrO in the coating increases. The relative ratio of SrTiO<sub>3</sub>/TiO<sub>2</sub> in the 10% SrO-TiO<sub>2</sub>, 20% SrO-TiO<sub>2</sub>, 30% SrO-TiO<sub>2</sub> coatings, calculated based on the relative peak intensity was 0.067, 0.246, 0.915, respectively. It is noted that with increase in the Sr amount in the coating, the intensity of diffraction peaks of rutile weakened, whereas those of anatase (25.3 $^{\circ}$ ) strengthened, indicating more anatase TiO<sub>2</sub> appeared in the SrO doped TiO<sub>2</sub> coatings.

Fig. 1 XRD patterns of the TiO<sub>2</sub> and SrO-TiO<sub>2</sub> coatings.

### 3.2. Morphology and structural characterization

The SEM images of the surface morphology of the TiO<sub>2</sub>-based coatings are shown in Fig. 2. All the coatings show a typical morphology of a plasma sprayed coating, having a rough surface with a surface roughness of 4–6  $\mu\text{m}$  (Fig. 2A–D). No significant difference was found among the TiO<sub>2</sub>, 10% SrO-TiO<sub>2</sub>, 20% SrO-TiO<sub>2</sub> and 30% SrO-TiO<sub>2</sub> coatings.

### 3.3. Electrochemical measurements

Fig. 3 displays the potentiodynamic polarization curves of the TiO<sub>2</sub>, 10% SrO-TiO<sub>2</sub>, 20% SrO-TiO<sub>2</sub> and 30% SrO-TiO<sub>2</sub> coatings in SBF solution. The corrosion potential ( $E_{\text{corr}}$ ), corrosion current density ( $I_{\text{corr}}$ ) and corrosion rate of the films calculated based on the polarization curves are listed in Table 2. The 20% SrO-TiO<sub>2</sub> coating (−573.7 mV) and the TiO<sub>2</sub> coating (−570.34 mV) have a comparable  $E_{\text{corr}}$ , which is less negative than those of the 10% SrO-TiO<sub>2</sub> (−599.7 mV) coating. The  $I_{\text{corr}}$  of the 20% SrO-TiO<sub>2</sub> coating (1.92  $\mu\text{A cm}^{-2}$ ) is slightly lower than that of the 10% SrO-TiO<sub>2</sub> coating (2.06  $\mu\text{A cm}^{-2}$ ), but obviously higher than that of the TiO<sub>2</sub> coating (2.70  $\mu\text{A cm}^{-2}$ ). The corrosion rate calculated based on the  $I_{\text{corr}}$  has the same tendency. Compared to other coatings, the 30% SrO-TiO<sub>2</sub> coating has the most negative  $E_{\text{corr}}$  (−1048.5 mV) and the highest  $I_{\text{corr}}$  (7.90  $\mu\text{A cm}^{-2}$ )/corrosion rate. These results suggest that the 20% SrO-TiO<sub>2</sub> coating has the best corrosion resistance while the 30% SrO-TiO<sub>2</sub> coating has the worst. It was reported that a lower point of zero charge (PZC) of materials exhibits a higher pitting potential and better corrosion resistance.<sup>26–29</sup> It was found that the PZC of SrTiO<sub>3</sub> is around 8.5–9.5, higher than that of TiO<sub>2</sub> (5–7),<sup>27</sup> which could be one of the possible reasons for the deteriorated corrosion resistance of the 30% SrO-TiO<sub>2</sub> coating. In addition, the corrosion resistance of the coating is also strongly influenced by the structural defects, such as microcracks and pores *etc.* Future work will be carried to investigate into the influence of the amount of Sr on the microstructures of the SrO-TiO<sub>2</sub> coatings.



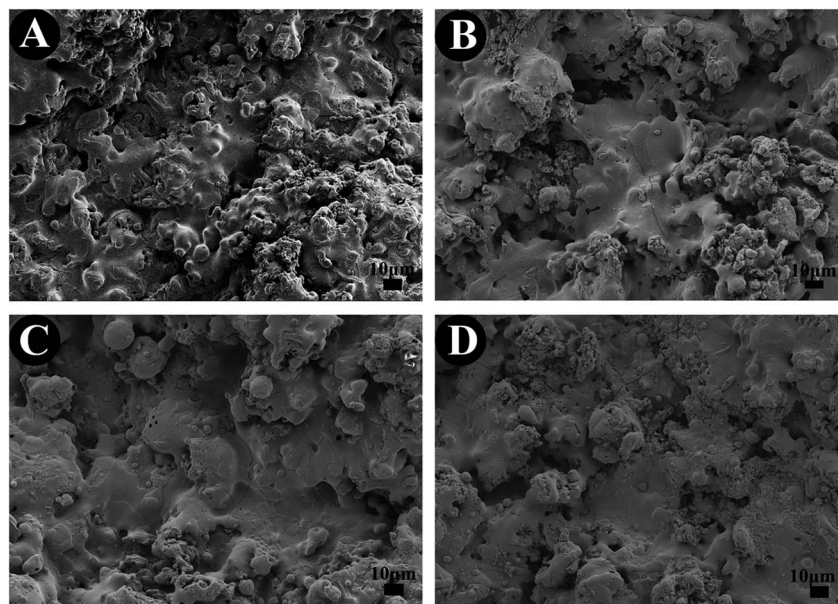


Fig. 2 SEM images of the TiO<sub>2</sub> (A), 10% SrO–TiO<sub>2</sub> (B), 20% SrO–TiO<sub>2</sub> (C) and 30% SrO–TiO<sub>2</sub> (D) coatings.

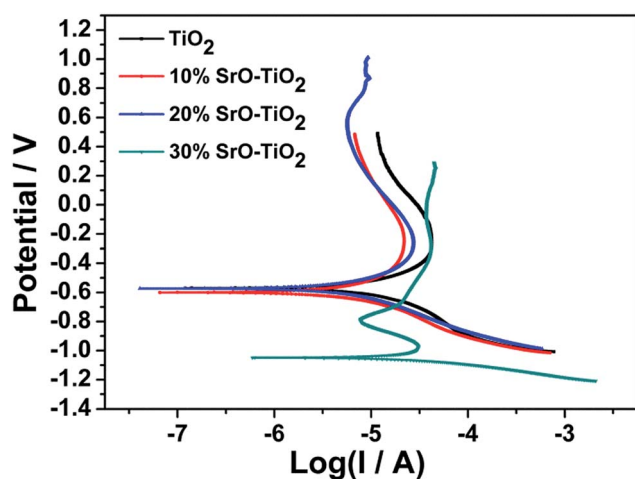


Fig. 3 Potentiodynamic polarization curves of TiO<sub>2</sub>, 10% SrO–TiO<sub>2</sub>, 20% SrO–TiO<sub>2</sub>, 30% SrO–TiO<sub>2</sub> coatings.

Table 2  $E_{\text{corr}}$ ,  $I_{\text{corr}}$  and corrosion rate of the coatings

| Sample                   | $E_{\text{corr}}$ (mV) | $I_{\text{corr}}$ ( $\mu\text{A cm}^{-2}$ ) | Corrosion rate (mm per year) |
|--------------------------|------------------------|---|------------------------------|
| TiO <sub>2</sub>         | −570.34                | 2.6971                                      | 0.09363                      |
| 10% SrO–TiO <sub>2</sub> | −599.7                 | 2.0559                                      | 0.071371                     |
| 20% SrO–TiO <sub>2</sub> | −573.7                 | 1.9233                                      | 0.066768                     |
| 30% SrO–TiO <sub>2</sub> | −1048.5                | 7.8986                                      | 0.2742                       |

### 3.4. *In vitro* mineralization

Fig. 4 represents the surface morphologies of the TiO<sub>2</sub>, 10% SrO–TiO<sub>2</sub>, 20% SrO–TiO<sub>2</sub> and 30% SrO–TiO<sub>2</sub> coatings after immersion in 2× SBF for 14 days. A large amount of granular precipitation is observed on the TiO<sub>2</sub>, 10% and 20% SrO–TiO<sub>2</sub> coatings, while few

observed on the 30% SrO–TiO<sub>2</sub> coating. Under higher magnifications, it can be seen that the precipitated granules consist of nanosized plate-like crystals. EDS results prove that the precipitation is mainly composed of Ca and P (top left insets). On the TiO<sub>2</sub> coating, the precipitation almost covers the whole surface, showing the best ability to induce *in vitro* mineralization. Among the SrO doped TiO<sub>2</sub> coatings, the amount of precipitation formed on the 10% SrO–TiO<sub>2</sub> coating seems the largest, followed by the 20% SrO–TiO<sub>2</sub> coating. Fig. 5 shows XRD results of the coatings soaked in 2× SBF for 14 days. The characteristic peaks at 25.8° and 31.6° corresponding to hydroxyapatite were observed in the XRD patterns, indicating that the newly formed precipitate was hydroxyapatite. In addition, the relative intensity ratio of HAP to TiO<sub>2</sub> is also found to decrease inversely with the Sr amount, consistent with what we observed from the SEM images (Fig. 4). These results suggest that the addition of SrO compromises the ability of the TiO<sub>2</sub> coating to induce apatite formation. Further work will be carried to illustrate the underlying mechanisms.

### 3.5. Ion release profile in culture medium

The Sr ion release behavior of the TiO<sub>2</sub>, 10% SrO–TiO<sub>2</sub>, 20% SrO–TiO<sub>2</sub> and 30% SrO–TiO<sub>2</sub> coatings were evaluated over 9 days and the release profile is shown in Fig. 6. It can be seen that Sr is releasable in all the doped TiO<sub>2</sub> coatings, and its concentration in the immersion medium increases as the immersion time extended from 3 days to 9 days (Fig. 6A). As shown in Fig. 6B, the Sr concentration at each times for the SrO doped TiO<sub>2</sub> coating is linearly related to the relative amount of SrO in the starting composite powders.

### 3.6. Cell adhesion and morphology

Fig. 7A shows fluorescence microscope images of the cell cultured on the Ti6Al4V, TiO<sub>2</sub>, 10% SrO–TiO<sub>2</sub>, 20% SrO–TiO<sub>2</sub>



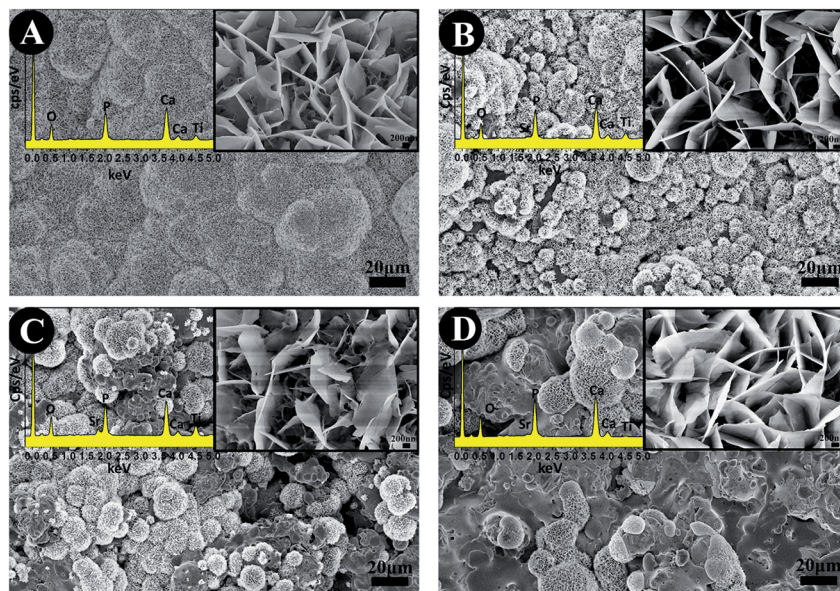


Fig. 4 The surface morphology of the TiO<sub>2</sub> (A), 10% SrO–TiO<sub>2</sub> (B), 20% SrO–TiO<sub>2</sub> (C), 30% SrO–TiO<sub>2</sub> (D) coatings after immersion in 2× SBF for 14 days.

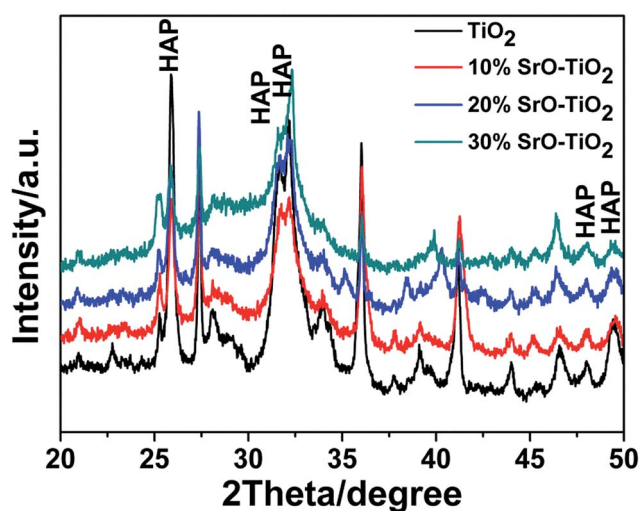


Fig. 5 XRD patterns of the TiO<sub>2</sub> coating and the SrO–TiO<sub>2</sub> coatings soaked in 2× SBF for 14 days.

and 30% SrO–TiO<sub>2</sub> coatings for 24 h. Cells on all the coatings get flattened and well attach to their underlying substrates. Among these coatings, the cells cultured on the 10% SrO–TiO<sub>2</sub> coating and the 20% SrO–TiO<sub>2</sub> coating, especially the latter one, exhibit distinct and well-defined stress fibers and cytoskeleton.

Fig. 7B shows the SEM images of the cells cultured on the samples for 24 h. Most of the cells on the Ti, TiO<sub>2</sub>, 10% SrO–TiO<sub>2</sub> and 20% SrO–TiO<sub>2</sub> coatings exhibit a flattened polygonal shapes, while those on the 30% SrO–TiO<sub>2</sub> coatings are less flattened.

### 3.7. Cell viability and proliferation

Cell proliferation results are shown in Fig. 8A. At day 3, cells cultured on the 20% SrO–TiO<sub>2</sub> coatings show higher

proliferation rates than those cultured on the TiO<sub>2</sub>, 10% SrO–TiO<sub>2</sub> and 30% SrO–TiO<sub>2</sub> coating. After culturing for 7 days, the proliferation rate of the cells on the 20% SrO–TiO<sub>2</sub> coating is still the highest, followed by that on the 10% SrO–TiO<sub>2</sub> coating, while the cells on the 30% SrO–TiO<sub>2</sub> coating exhibit the lowest proliferation rate. The average proliferation rate for the cells on the TiO<sub>2</sub> coating is higher than that on the Ti6Al4V, but without significant statistic difference. These results indicate that Sr doping has great effects on the cell proliferation on the coatings and the 20% SrO–TiO<sub>2</sub> coating has the best positive effect.

### 3.8. Alkaline phosphatase (ALP) activity

Fig. 8B shows the ALP activity of the cells cultured on the Ti6Al4V, the TiO<sub>2</sub>, 10% SrO–TiO<sub>2</sub>, 20% SrO–TiO<sub>2</sub>, 30% SrO–TiO<sub>2</sub> coatings at day 14. It can be seen that the ALP activity of the cells cultured on the 10% SrO–TiO<sub>2</sub> coating and the 20% SrO–TiO<sub>2</sub> coating is comparable, which is significantly higher than those for the cells on the Ti6Al4V and the TiO<sub>2</sub> coating. The ALP activity of the cells on the 30% SrO–TiO<sub>2</sub> coating is lowest.

### 3.9. mRNA expression of the osteogenic-related genes

Fig. 9 displays the expression of the osteogenic-related genes by the cells cultured on the Ti6Al4V, the TiO<sub>2</sub> coating, and the Sr-doped TiO<sub>2</sub> coatings. Among these genes, RUNX-2 and COL-1 are early markers, while OCN and OPN are later markers for osteogenic differentiation. As shown in Fig. 9, after 7 days, the COL-1 expression levels by the cells cultured on the TiO<sub>2</sub> coating, the 10% SrO–TiO<sub>2</sub> coating and the 20% SrO–TiO<sub>2</sub> coating are significantly higher than those on the Ti6Al4V and the 30% SrO–TiO<sub>2</sub> coating. At day 14, the COL-1 expression level on the 20% SrO–TiO<sub>2</sub> coating become the highest, which nearly doubles those for the other coatings. For OCN, no difference is found for all the samples at day 7. However, the cells cultured



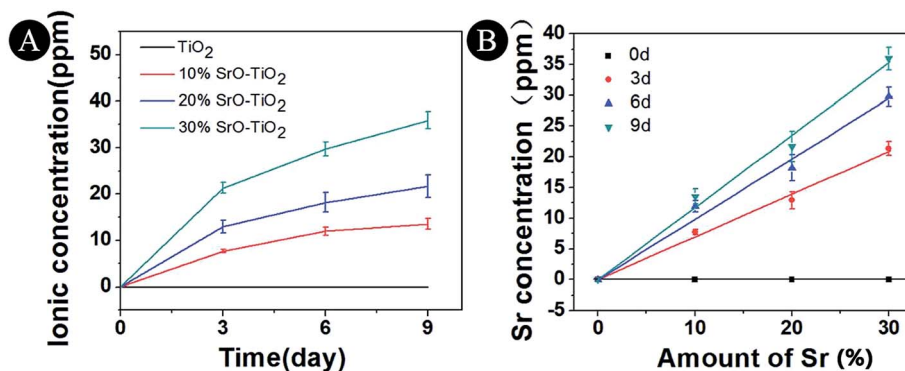


Fig. 6 Concentrations of Sr ions released from TiO<sub>2</sub>, 10% SrO-TiO<sub>2</sub>, 20% SrO-TiO<sub>2</sub>, 30% SrO-TiO<sub>2</sub> coatings after immersion in culture medium for 3, 6 and 9 days.

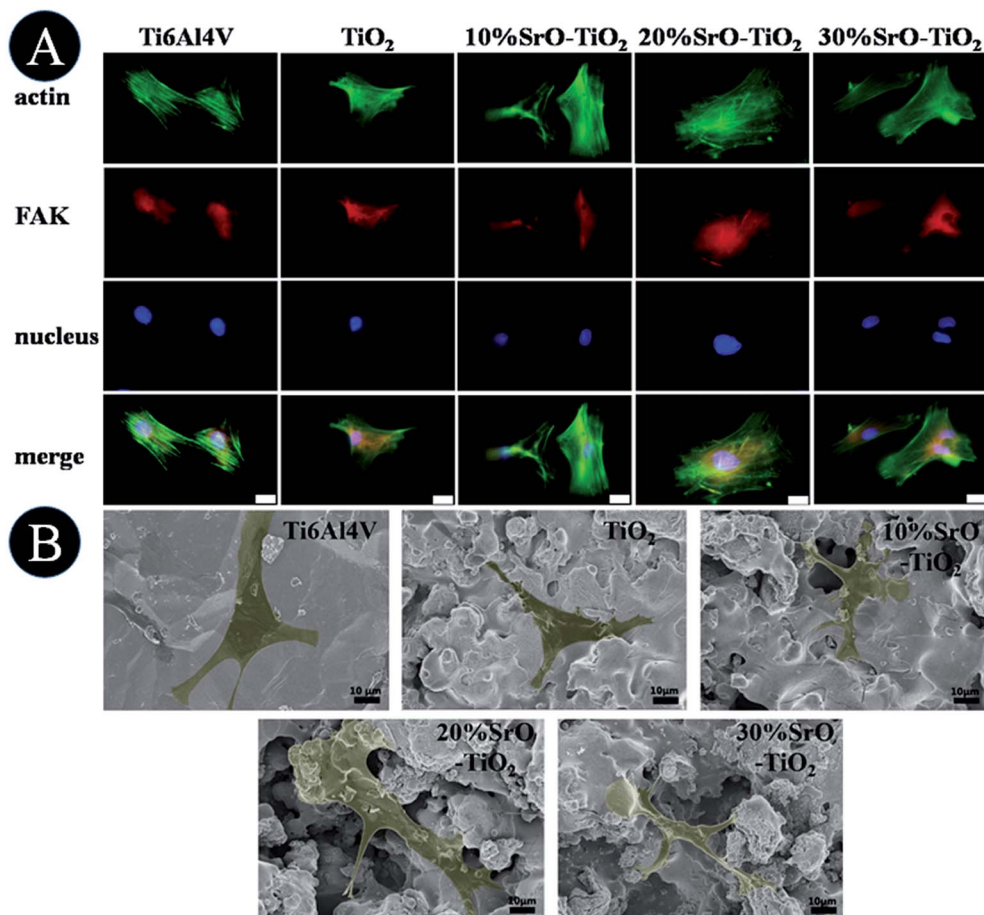


Fig. 7 Observation of cell initial attachment on the coatings, fluorescence microscope images (A) and SEM (B) of cells cultured on Ti6Al4V, TiO<sub>2</sub>, 10% SrO-TiO<sub>2</sub>, 20% SrO-TiO<sub>2</sub>, 30% SrO-TiO<sub>2</sub> for 24 h. Scale bar, 20 μm.

on the 20% SrO-TiO<sub>2</sub> coating display the highest OCN expression level at day 14 and no significant difference can be seen between the 10% SrO-TiO<sub>2</sub> coating and the 30% SrO-TiO<sub>2</sub> coating. For OPN, its levels expressed by the cells on the 10% SrO-TiO<sub>2</sub> coating and the 20% SrO-TiO<sub>2</sub> coating are comparable and significantly higher than those for the other coatings at day 7. After culturing for 14 days, no significant difference

can be found anymore between the 10% SrO-TiO<sub>2</sub> coating and 20% SrO-TiO<sub>2</sub> coating, but their expression levels are higher than the control groups. For RUNX-2, at both day 7 and 14, its expression levels by the cells cultured on the 10% SrO-TiO<sub>2</sub> coating and the 20% SrO-TiO<sub>2</sub> coating are comparable and higher than those by the cells on the control groups. Again, the cells cultured on the 30% SrO-TiO<sub>2</sub> coating show the lowest



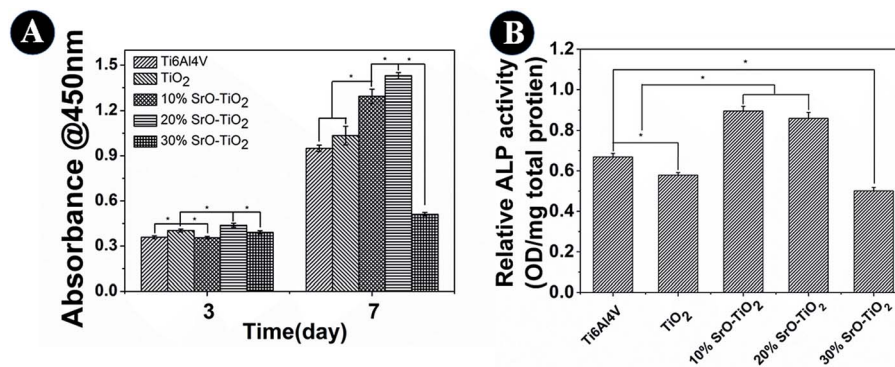


Fig. 8 The proliferation and ALP activity and of rBMSCs cultured on the Ti6Al4V, TiO<sub>2</sub>, 10% SrO–TiO<sub>2</sub>, 20% SrO–TiO<sub>2</sub>, 30% SrO–TiO<sub>2</sub> coatings at day 14.

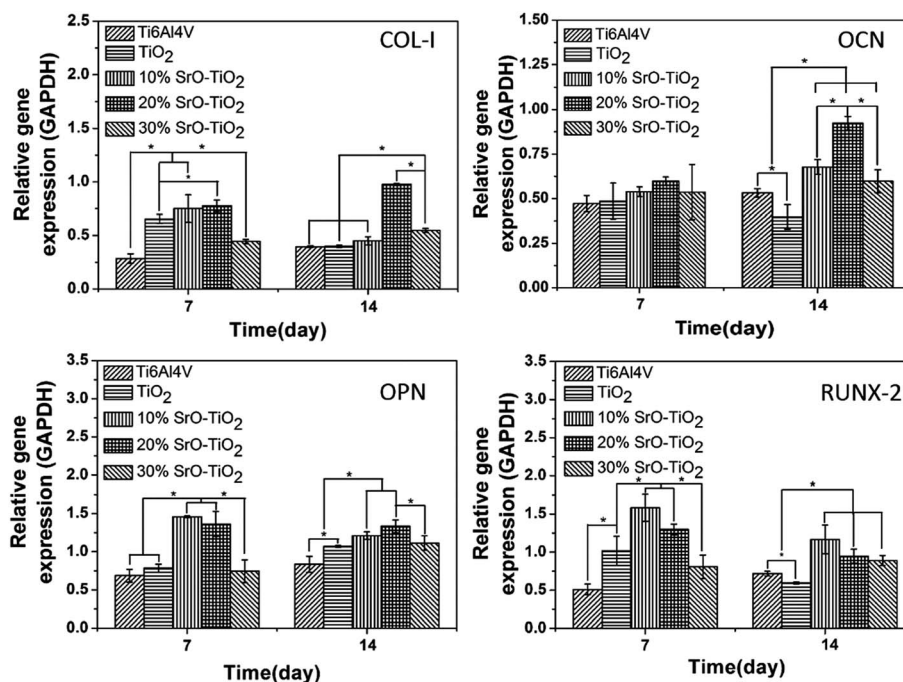


Fig. 9 Quantitative PCR analysis of the cells cultured on TiO<sub>2</sub>, 10% SrO–TiO<sub>2</sub>, 20% SrO–TiO<sub>2</sub>, 30% SrO–TiO<sub>2</sub> coatings for 7 and 14 days, house-keeping gene GAPDH was used as an internal control. \*Statistically significant difference among different samples ( $p < 0.05$ ).

expression level. In general, it can be concluded from these results that the 20% SrO–TiO<sub>2</sub> coating are superior to the others in promoting osteogenic differentiation, while the 30% SrO–TiO<sub>2</sub> coating showed obviously less osteogenic activity compared to the other doped coatings.

## 4. Discussion

In this study, we developed SrO–TiO<sub>2</sub> coatings to enhance the osseointegration of the metallic orthopaedic implant. Compared to the commonly used biodegradable Sr-containing biomedical coating,<sup>30–34</sup> the combination of bioactive Sr and non-degradable TiO<sub>2</sub> in this study endowed the coating with an ability to release bioactive Sr (Fig. 6) and thus obviously improving the osteogenic activity (Fig. 9). It should be noted

that the release of Sr is not combined with the release of Ti, indicating that the release of Sr in the developed coating system is selective, which will benefit the long-term stability of the implant.

In the SrO-doped TiO<sub>2</sub> coatings, the Sr exists in two different configurations: Sr intercalated in TiO<sub>2</sub> lattice and SrTiO<sub>3</sub>. In the 10% SrO–TiO<sub>2</sub> coating, the amount of SrTiO<sub>3</sub> calculated from XRD patterns is around 6.31 wt%. The atomic ratio of the Sr in the SrTiO<sub>3</sub> relative to the total amount of Ti in this coating is 0.017, much less than the theoretic value of 0.052, suggesting that there must be some part of Sr (0.035) existing in other configurations. Based on the solid solution and doping theory, the most possible configuration of Sr is as interstitial atoms of the TiO<sub>2</sub> lattice in SrO–TiO<sub>2</sub> solid solution (Fig. 1). When the SrO amount increases to 20%, the percent of SrTiO<sub>3</sub> is around



19.7 wt%, leading to a Sr/Ti of 0.061, which is nearly half of the theoretic value (0.115). Therefore, there are also a large part of Sr existing as an interstitial solute in the SrO–TiO<sub>2</sub> solid solution.<sup>35,36</sup> However, in the 30% SrO–TiO<sub>2</sub> coating, the ratio of Sr in SrTiO<sub>3</sub> relative to the total Ti in the coating (0.193) is very close to the theoretic value (0.198), therefore, it can be concluded that Sr in this coating exists only in the form of SrTiO<sub>3</sub>. Therefore, the ion release of Sr from the SrO-doped TiO<sub>2</sub> coating is contributed by two different Sr configurations. For the 10% SrO–TiO<sub>2</sub> coating and the 20% SrO–TiO<sub>2</sub> coating, the released Sr is from both SrTiO<sub>3</sub> and the Ti<sub>y</sub>Sr<sub>2–2y</sub>O<sub>2</sub> solid solution, whereas that for the 30% SrO–TiO<sub>2</sub> coating is solely from SrTiO<sub>3</sub>. As shown in Fig. 6, the linear release behavior was achieved for all the coatings by the two Sr configurations, suggesting that the Sr release could be precisely controlled by adjusting the amount of Sr and the Sr configurations in the coating. However, it should be noted that there are numerous nanosized crystals precipitated on the surface of the 30% SrO–TiO<sub>2</sub> coating after incubation with cells for 24 h, as shown in Fig. 10A. Based on the EDS results, the Sr/Ti ratio of the newly formed crystals is around 0.45, nearly doubles the theoretical value of 0.19, implying that the newly formed crystals is a Sr-rich compound. Based on this, it can be deduced that the Sr released from the 30% SrO–TiO<sub>2</sub> coating possibly led to an increased supersaturation degree with respect to a certain of Sr-containing compound, which “recycles” the released Sr ions, and ultimately decreased the ion concentration in their extracts.<sup>37</sup> Therefore, the linear release behavior for the 30% SrO–TiO<sub>2</sub> with respect to the SrO amount is also contributed by the newly formed layer of the crystals.

The TiO<sub>2</sub> powders we used in this study are composed of 85% anatase and 15% rutile TiO<sub>2</sub>. However, it can be seen that the relative amount of the anatase TiO<sub>2</sub> was significantly reduced after plasma spraying, indicating that plasma spraying promotes the phase transformation from anatase to rutile (Fig. 10B). With the increase in the amount of Sr in the coating, the relative amount of the anatase TiO<sub>2</sub> increases, applying that the Sr incorporation can suppress the anatase to rutile transformation. It is well-known that rutile and anatase are two most common phases for TiO<sub>2</sub>.<sup>38</sup> V. Sollazzo reported that anatase TiO<sub>2</sub> has better bioactivity compared to the rutile phase.<sup>39</sup> Although no direct evidence is obtained in this study to prove the contribution of the anatase TiO<sub>2</sub> on the bioactivity, the rutile to anatase transformation caused by Sr doping still could be a merit of our coating design, which might provide some guidance for further biomedical coating design based on the TiO<sub>2</sub> material. Based on the biological results, we found that the 20% SrO–TiO<sub>2</sub> coating not only promoted the proliferation of rBMSCs (Fig. 8A), but also enhanced their osteogenic differentiation, as indicated in the ALP activity (Fig. 8B) and gene expression levels (Fig. 9), which is closely related to the Sr ions released from the coating. To illustrate the dominant effects of the Sr ion on the enhancement of the osteogenic activity, we used the extract of the samples to culture the rBMSCs to evaluate the biological effects of the dissolution products. The expression levels of bone-related genes (OPN, RUNX-2, COL-1 and OCN) by the cells cultured for 7 days in the extracts were presented in Fig. 10C. It can be seen that the cells cultured by the extract of the 20% SrO–TiO<sub>2</sub> coating express the highest levels of these genes, whereas those cultured in the extract of

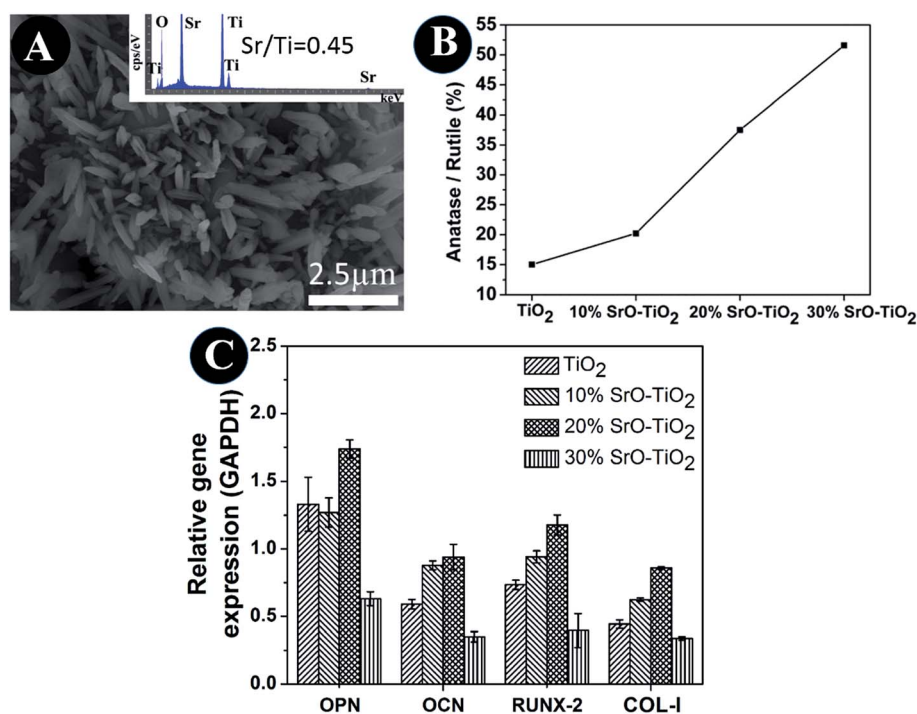


Fig. 10 SEM and EDS of crystals precipitated on its surface after incubation with cells for 24 h (A), the ratio of anatase and rutile phase in the composite coatings (B), quantitative PCR analysis of the cells cultured on TiO<sub>2</sub>, 10% SrO–TiO<sub>2</sub>, 20% SrO–TiO<sub>2</sub>, 30% SrO–TiO<sub>2</sub> coatings dissolution products (C).



the 30% SrO–TiO<sub>2</sub> coating express the lowest levels. The consistency of the gene expression results for the cells directly cultured on the coating surface and incubated with the coating extracts further validates the importance of Sr ions for the osteogenic activity. Similar to the biological drugs, the effects of the bioactive ions are also dose-dependent.<sup>10,40,41</sup> Therefore, based on the biological results, we may conclude that the Sr ions released from the 20% SrO–TiO<sub>2</sub> coating is the optimal and the Sr ions from the 30% SrO–TiO<sub>2</sub> coating are possibly overdosed.

## 5. Conclusion

In summary, non-degradable bioactive coating was designed based a SrO–TiO<sub>2</sub> system in this work, which is able to selectively release Sr ions. It was proven that the release of Sr ions is dependent on the Sr configurations in the coating, which has great influence on the osteogenic activity of the bone cells. Sr mainly exists as interstitial atoms in a solid solution of Ti<sub>y</sub>–Sr<sub>2–2y</sub>O<sub>2</sub> when its amount is less than 10 wt%, and only SrTiO<sub>3</sub> configuration appears when the Sr amount is higher than 30%. Both configurations present in the coatings with a Sr amount lying in between. We found that the addition of Sr compromises the *in vitro* mineralization ability of the TiO<sub>2</sub> coating, inversely proportional to its amount. However, its beneficial effects on osteogenesis enhancement are prominent. It was proved that the 20% SrO–TiO<sub>2</sub> coating shows the best capacity of enhancing cellular proliferation and osteogenic differentiation, pointing out its potential application as an orthopaedic implant coating.

## Conflicts of interest

There are no conflicts to declare.

## Acknowledgements

The authors would like to acknowledge funding support from Shenzhen Science and Technology Research funding (JCYJ20150630114942256, JSGG20151030140325149, JCYJ20170413161800287), the Guangdong Provincial Science and Technology Project (2017A010103014) and National Natural Science Foundation (31700835). The authors also want to thank the final support from the Shenzhen Peacock Innovation Team (Grant 110811003586331).

## References

- C. Andreini, I. Bertini, G. Cavallaro, G. L. Holliday and J. M. Thornton, *J. Biol. Inorg. Chem.*, 2008, **13**, 1205–1218.
- A. Budimir, *Acta Pharm.*, 2011, **61**, 1–14.
- V. Mouriño, J. P. Cattalini and A. R. Boccacini, *J. R. Soc., Interface*, 2012, **9**, 401–419.
- N. A. T. Hamdy, *Rheumatology*, 2009, **48**, 9–13.
- H. Hu, W. Zhang, Y. Qiao, X. Jiang, X. Liu and C. Ding, *Acta Biomater.*, 2012, **8**, 904–915.
- Z. Chen, X. Mao, L. Tan, T. Friis, C. Wu, R. Crawford and Y. Xiao, *Biomaterials*, 2014, **35**, 8553–8565.
- N. J. Lakhkar, I. H. Lee, H. W. Kim, V. Salih, I. B. Wall and J. C. Knowles, *Adv. Drug Delivery Rev.*, 2013, **65**, 405–420.
- Z. Saidak and P. J. Marie, *Pharmacol. Ther.*, 2012, **136**, 216–226.
- L. Zhao, H. Wang, K. Huo, X. Zhang, W. Wang, Y. Zhang, Z. Wu and P. K. Chu, *Biomaterials*, 2013, **34**, 19–29.
- J. W. Park, H. K. Kim, Y. J. Kim, J. H. Jang, H. Song and T. Hanawa, *Acta Biomater.*, 2010, **6**, 2843–2851.
- M. Long and H. J. Rack, *Biomaterials*, 1998, **19**, 1621–1639.
- W. Yang, X. Xi, Y. Si, S. Huang, J. Wang and K. Cai, *Acta Biomater.*, 2014, **10**, 4525–4536.
- L. L. Guéhenec, A. Soueidan, P. Layrolle and Y. Amouriq, *Dent. Mater.*, 2007, **23**, 844–854.
- H. Schliephake and D. Scharnweber, *J. Mater. Chem.*, 2008, **18**, 2404–2414.
- J. W. Park, H. K. Kim, Y. J. Kim, J. H. Jang, H. Song and T. Hanawa, *Acta Biomater.*, 2010, **6**, 2843–2851.
- W. Zhang, G. Wang, Y. Liu, X. Zhao, D. Zou, C. Zhu, Y. Jin, Q. Huang, J. Sun, X. Liu, X. Jiang and H. Zreiqat, *Biomaterials*, 2013, **34**, 3184–3195.
- C. Wu, Y. Ramaswamy, D. Kwik and H. Zreiqat, *Biomaterials*, 2007, **28**, 3171–3181.
- O. Z. Andersen, V. Offermanns, M. Sillassen, K. P. Almqvist, I. H. Andersen, S. Sørensen, C. S. Jeppesen, D. C. E. Kraft, J. Böttiger, M. Rasse, F. Kloss and M. Foss, *Biomaterials*, 2013, **34**, 5883–5890.
- J. Lao, J. M. Nedelec and E. Jallot, *J. Mater. Chem.*, 2009, **19**, 2940–2949.
- Y. Dang, L. Zhang, W. Song, B. Chang, T. Han, Y. Zhang and L. Zhao, *Int. J. Nanomed.*, 2016, **11**, 1003–1011.
- H. Zreiqat, Y. Ramaswamy, C. Wu, A. Paschalidis, Z. Lu, B. James, O. Birke, M. McDonald, D. Little and C. R. Dunstan, *Biomaterials*, 2010, **31**, 3175–3184.
- K. Søballe and S. Overgaard, *J. Bone Joint Surg Br*, 1996, **78**, 689–691.
- T. Kokubo and H. Takadama, *Biomaterials*, 2006, **27**, 2907–2915.
- M. Stern, *Corrosion*, 1958, **14**, 60–64.
- G. Wang, Z. Lu, D. Dewart and H. Zreiqat, *Mater. Sci. Eng., C*, 2012, **32**, 1818–1826.
- P. M. Natishan, E. McCafferty, G. K. Hubler and J. E. Soc, *J. Electrochem. Soc.*, 1988, **135**, 321.
- M. Kosmulski, *J. Colloid Interface Sci.*, 2009, **337**, 439–448.
- M. Kosmulski, *J. Colloid Interface Sci.*, 2011, **353**, 1–15.
- M. Kosmulski, *J. Colloid Interface Sci.*, 2014, **426**, 209–212.
- C. Capuccini, P. Torricelli, E. Boanini, M. Gazzano, R. Giardino and A. Bigi, *J. Biomed. Mater. Res., Part A*, 2009, **89**, 594–600.
- S. D. Newman, N. Lotfibakhshaiesh, M. O'Donnell, X. F. Walboomers, N. Horwood, J. A. Jansen, A. A. Amis, J. P. Cobb, M. M. Stevens, M. O. Donnell, X. F. Walboomers, N. Horwood, J. A. Jansen, A. A. Amis, J. P. Cobb and M. M. Stevens, *Tissue Eng., Part A*, 2014, **20**, 1850–1857.
- L. Li, X. Lu, Y. Meng and C. M. Weyant, *J. Mater. Sci.: Mater. Med.*, 2012, **23**, 2359–2368.



- 33 X. Wang, Z. Gu, B. Jiang, L. Li and X. Yu, *Biomater. Sci.*, 2016, **4**, 678–688.
- 34 S. Omar, F. Repp, P. M. Desimone, R. Weinkamer, W. Wagermaier, S. Ceré and J. Ballarre, *J. Non-Cryst. Solids*, 2015, **425**, 1–10.
- 35 D. Wu, F. Mao, Z. Yang, S. Wang and Z. Zhou, *Mater. Sci. Semicond. Process.*, 2014, **23**, 72–77.
- 36 A. Alem and H. Sarpoolaky, *Solid State Sci.*, 2010, **12**, 1469–1472.
- 37 G. Wang, X. Zhao, M. Möller and S. E. Moya, *ACS Appl. Mater. Interfaces*, 2015, **7**, 23412–23417.
- 38 J. Wang, J. Ge, H. Hou, M. Wang, G. Liu, G. Qiao and Y. Wang, *Appl. Surf. Sci.*, 2017, **422**, 970–974.
- 39 V. Sollazzo, F. Pezzetti, A. Scarano, A. Piattelli, L. Massari, G. Brunelli and F. Carinci, *J. Craniofac Surg*, 2007, **18**, 806–810.
- 40 P. J. Marie, P. Ammann, G. Boivin and C. Rey, *Calcif. Tissue Int.*, 2001, **69**, 121–129.
- 41 A. Hoppe, N. S. Güldal and A. R. Boccaccini, *Biomaterials*, 2011, **32**, 2757–2774.

